Dynamic and Static Loading Effects on Aircraft Avionics Support Structures

ES-202 Final Report

Kendall Pielin, Craig Slovensky, Clancy Crawford, Hayden O’Shea

Introduction:

Aircraft are subject to a wide range of mechanical loads throughout their operational cycle, including while parked, taxiing, accelerating, cruising, encountering turbulence, and landing. Each of these phases introduces unique stresses to the aircraft's structure, from static gravitational loads to dynamic inertial and vibrational forces. These stresses are not only critical to the structural integrity of the aircraft as a whole but are especially significant for internal support systems, such as those securing avionics boxes and other sensitive components. Understanding how these loads interact with mounting structures is essential to ensuring long-term safety, performance, and durability.

In real-world engineering, the principles of solid mechanics are applied to quantify these forces and design structures capable of withstanding them. This project applies those theoretical concepts—such as shear and bending moment analysis, stress transformation, and inertial force modeling—to a practical case study involving an avionics box mounted within an F-22 jet, allowing us to evaluate its behavior under typical and extreme loading scenarios.

Throughout the aircraft's operation, each phase introduces unique mechanical stresses that must be considered in the design of internal support structures. As the aircraft accelerates for takeoff, dynamic forces such as drag, vibration, and inertial loading increase, placing additional stress on components like avionics mounts. During flight, turbulence can momentarily alter the effective weight on structures due to rapid vertical and lateral accelerations, leading to fluctuating stress cycles. Landing produces the highest loads, with both vertical g-forces from touchdown and horizontal forces from braking combining to test the strength and stability of all support systems. Understanding and accounting for these loads is essential to ensure that mounting systems maintain integrity and safety under all expected operating conditions.

Objective:

The primary objective of this project is to analyze and quantify the forces acting on a mounting structure within an aircraft—specifically an avionics box—across various flight conditions including parked (static), taxiing, takeoff, level flight, turbulence, and landing. The project focuses on identifying and categorizing all relevant structural loads, and calculating the effects of acceleration, vibration, and aerodynamic forces on the mounting system. To support this analysis, shear and bending moment diagrams were developed for each phase of flight. Additionally, stress concentrations and transformations were evaluated using both analytical methods and computational tools. The final goal was to determine whether the

material properties and structural design of the support system are sufficient to withstand the maximum expected loading conditions throughout the aircraft's operation.

Approach:

To meet the objectives of the project, a structured approach was followed, beginning with a comprehensive research phase. This phase involved reviewing relevant aerospace engineering literature, FAA guidelines, and structural dynamics principles to understand the different types of loads an aircraft experiences, their magnitudes, and how these loads impact mounting structures.

Following the research, the modeling and design phase began, where a CAD model of the mounting structure was created using SolidWorks. This model allowed for the analysis of the geometry, material properties, and mass distribution of the mounting system. Subsequently, various load cases were defined, including static loads, dynamic loads, and environmental factors such as turbulence and wind. These load cases were crucial for simulating realistic operational conditions.

The next phase focused on force and stress analysis, which involved both manual calculations and SolidWorks simulations to determine internal forces, moments, and stress distributions within the mounting system. Shear and moment diagrams were then developed to visualize the structural response across different flight phases, helping to further understand the behavior of the mounting structure under various loading conditions.

Stress transformation techniques were applied using Mohr's Circle to assess the principal and shear stresses under combined loading conditions. These transformations were essential to evaluating how the material would behave under complex forces. Finally, the computed stresses were compared to the material's limits to assess safety margins and failure risks in worst-case scenarios. The results were then interpreted in the context of solid mechanics theory, and real-world applications of academic concepts were discussed in the conclusion of the project.

Load Effects:

The flight stages considered in this project include takeoff, level flight, and landing. Each of these phases subjects the aircraft and its internal structures to distinct loading conditions, which vary in intensity and direction. By evaluating each stage, the design of the mounting structure for the avionics box can be assessed under a comprehensive range of operational scenarios, from minimal loads during static parking to extreme forces encountered during turbulent flight or hard landings.

During takeoff, the aircraft begins to experience dynamic loads, including drag, rolling resistance, and acceleration-induced inertial forces. In-flight turbulence introduces rapid, unpredictable changes in vertical and lateral acceleration, producing cyclical stress and potential vibration throughout the mounting system. Landing introduces the most significant vertical and horizontal loads due to the sudden impact with the runway and braking forces, often resulting in elevated g-forces.

Critical load effects were identified primarily during the landing and takeoff phases. These stages involve both the highest magnitudes of force and the most abrupt changes in direction. The most vulnerable locations in the mounting structure are at points of stress concentration—particularly near fasteners, joints, and support interfaces where bending moments and shear forces are highest. These areas must be carefully reinforced or redesigned to handle worst-case loading scenarios, ensuring the mounting system remains structurally sound across the aircraft's entire operational envelope.

Moment and Shear Diagrams for Level Flight:

The structure is assessed via its front and side views, as the box may be under any orientation during flight. These extremes should account for the whole flight envelope. During level flight the box does not experience significant loading in terms of the vertical. Therefore, the structure is only responsible for its own weight.

Side View:

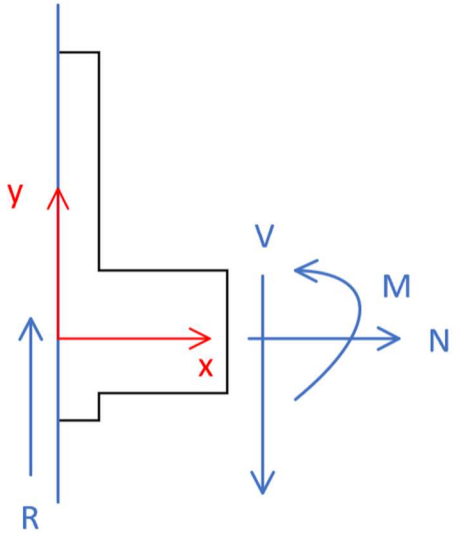

Weight = (5.103 kg)(-9.81 m/s^2)
= -50.06 N
=Max Shear Load

$\sum Fy = R + V$
$R = -V = 50.06$ N/m

Moment = (-50.06 N)(.5)(134.7)
= -7629.14 N/mm

Shear Diagram

(Max +ve)Shear Load (N): 50.060,

Location (mm): 0.000

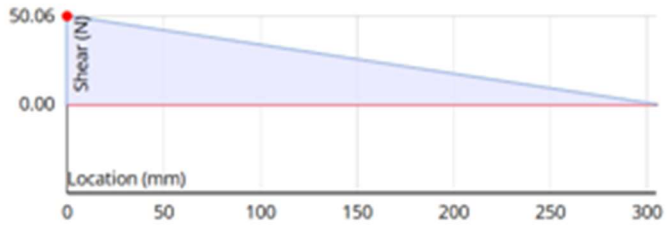

Moment Diagram

(Max -ve)Moment Load (N-mm): -7629.142,

Location (mm): 0.000

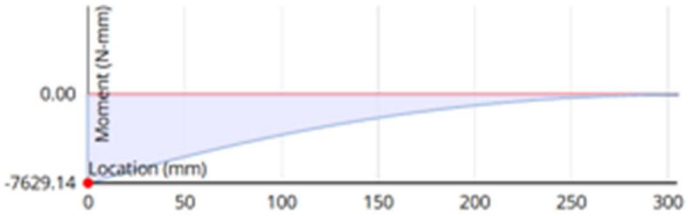

Front View:

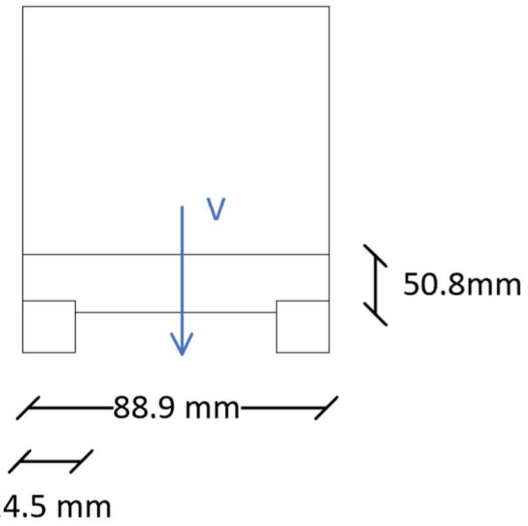

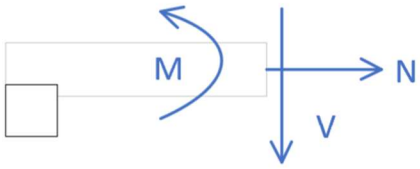

Method of Sections:

$\sum Fy = Ra + Rb - V$

$Ra + Rb = V$

$Ra = Rb \rightarrow 2R = V$

$2R = 50.06$

$R = 25.03\ N$

$M = (25.03N)(152.4mm/2)$

$= 1907.28\ N - mm^2$

Reaction forces are equal. Supports are same distance and magnitude from center.

Moment and Shear for takeoff:

During the first stage of takeoff, the supports experience lateral acceleration and the corresponding reactions fall to the normal direction. The forces coupled with this acceleration are derived from preexisting information considering the circumstances and conditions we are assuming. This diagram is the same as level flight.

During the second stage of takeoff, the aircraft inclines at varying angles. During this period the supports experience a great increase in the gravitational force acting on the system as well as the angular relation that the vertical forces have to the supports. Reaction forces become split into vertical and horizontal components in the effort to counterbalance the weight distribution.

Shear Diagram

(Max +ve)Shear Load (N): 25.030,

Location (mm): 0.000

(Max -ve)Shear Load (N): -25.030,

Location (mm): 304.800

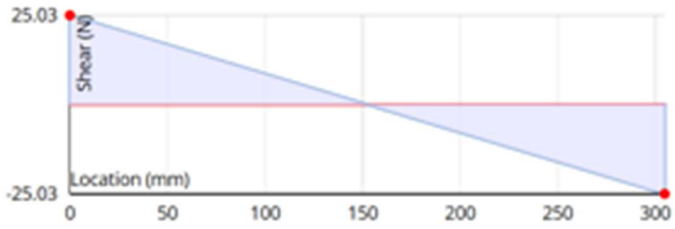

Moment Diagram

(Max +ve)Moment Load (N-mm): 1907.285,

Location (mm): 152.400

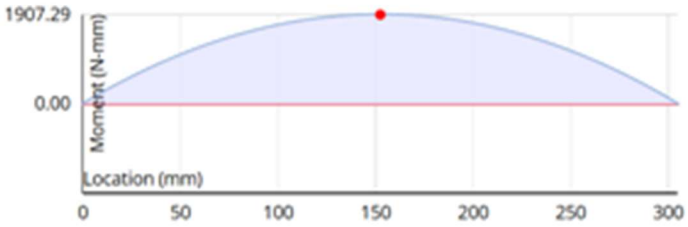

Shear Diagram

(Max +ve)Shear Load (kN): 26.314,

Location (mm): 0.000

(Max -ve)Shear Load (kN): -26.314,

Location (mm): 138.000

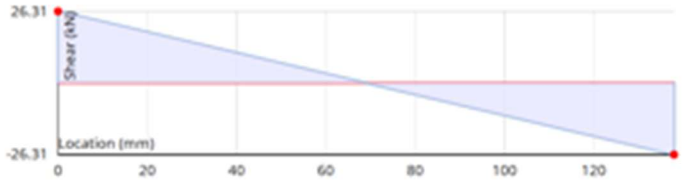

Moment Diagram

(Max +ve)Moment Load (kN-mm): 907.827,

Location (mm): 69.000

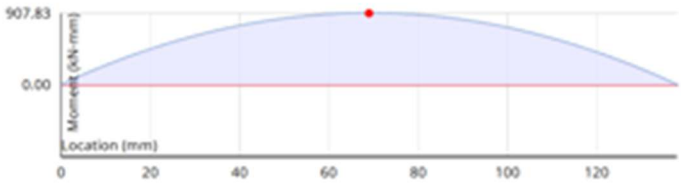

Front View:

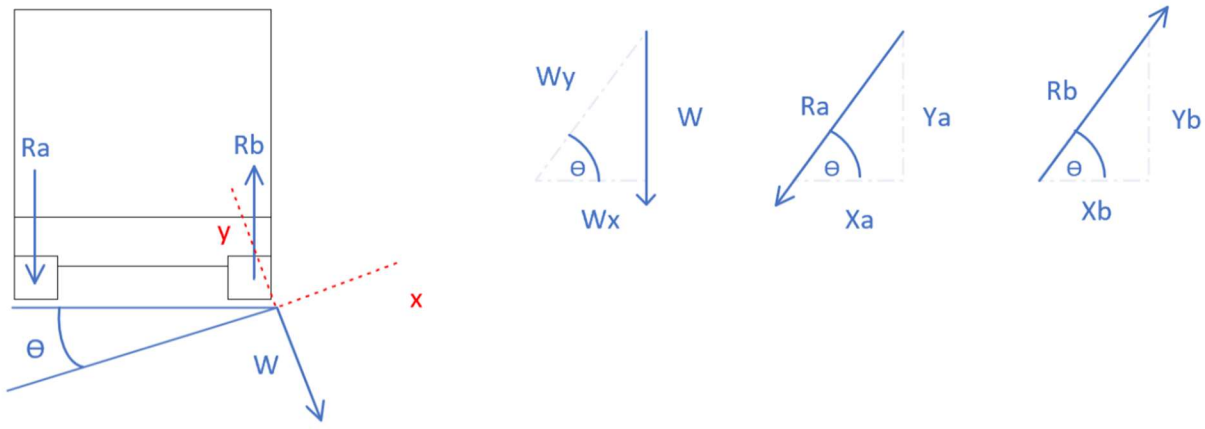

Moment and Shear Diagram Landing:

Landing procedures endure the same angular disparity as takeoff does, however the vital tradeoff is the downward acceleration that in fact reduces the downward force applied to the box. During this time the supports will not be under forces larger than the weight of the box while experiencing level glide or downward acceleration.

Shear Diagram

(Max +ve)Shear Load (N): 25.048,

Location (mm): 0.000

(Max -ve)Shear Load (N): -25.012,

Location (mm): 113.400, 138.000

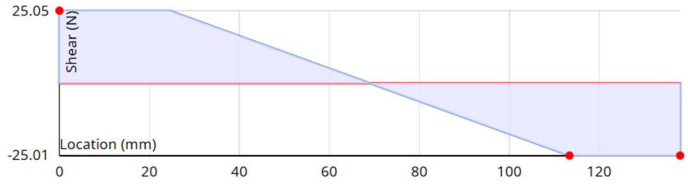

Moment Diagram

(Max +ve)Moment Load (N-mm): 1170.777,

Location (mm): 68.950

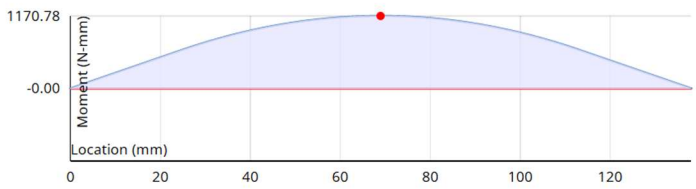

$\sum Fy = Ra + Rb - V$

$Ra + Rb = V$

$Ra = Rb \rightarrow 2R = V$

$2R = 50.06$

$R = 25.03\ N$

$M = (25.03N)(.67mm)(68.95mm)$

$= 1170.78\ N - mm^2$

Side View:

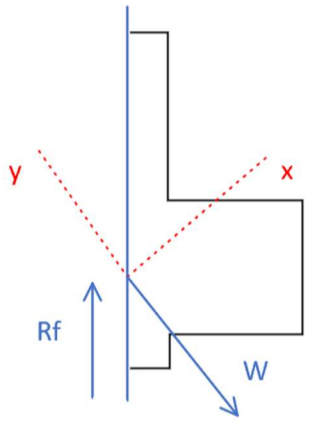

W = 50.06 N

sinΘ = W/Wy
Wy =W/sinΘ

tanΘ = W/Wx
Wx = W/tanΘ

$0 \leq Wy(\Theta) \leq 25.03$ N
$0 \leq Wx(\Theta) \leq 25.03$ N

The forces act in the same direction as takeoff and weight is still a function of theta.

In landing, the supports will not experience forces larger then the weight of the structure.

Overlooked factors:

During landing, these combined loads can significantly increase the force on mounting systems. For example, if an aircraft experiences 2.5g during touchdown, a component that weighs 100 N at rest could momentarily exert 250 N of force on its mounting structure. This increase must be accounted for in structural design and fatigue analysis to ensure safety and reliability. In reality the loading during landing, would be more significant due to G-Force factors.

Combined Loading:

To transition into the calculations of combined loading we took the internal force calculations and applied them to the cross section of the mount. This cross-section was derived from our cad design of the structure in solid works. Solid Works calculates the moment of inertia as part of the overall mass properties. It considers the objects shape, mass and axis of orientation.

The total normal stress at each stage of flight can be calculated using a combination of the axial stress and the bending moment. There is no axial stress present at any stage of flight, therefore this term is equal to zero. The total stress will simply be the sum of the bending moments. The shear stress at a specific point on the cross section of the beam. These values determine the intensity of internal forces.

These calculations were done at the points where the structure experiences the maximum moments. This should account for any stresses lesser than the max.

Overall, landing proves to be the most stressful state the structure will endure.

Takeoff:

$\sigma = N/A + Mc/I$
$= (1.8367)(.26162m)/(2926.8 \times 4.16 \times 10^{-7})$

$\sigma = 394.7$ kPA

The N/A term is =0 because there is no axial load in takeoff.

A' = 26.88 in^2 = .0173 m^2
ybar = 4.62 in
ybar' = .117 in
Center of mount = .26162 m

I = Moment of Inertia
= (2926.8)(4.16x10^7)in^4

*solid works given value

$Q = ybar' \times A'$

$= (.117\ m)(.0173\ m^2)$

$= .00306\ m^3$

$\tau = VQ / It$

$= (26.31\ kN)(.00306\ m^3) / (2926.8 \times 4.16 \times 10^{-7}\ m^4)(.26162\ m)$

$= 252.7$ MPa

Level Flight:

$$\sigma = N/A + Mc/I$$

$$= (.007629)(.26162) / (2926 \times 4.16 \times 10^{-7})$$

$$= 1.63 \text{ MPa}$$

$$\tau = (.051)(.00306) / ((2926 \times 4.16 \times 10^{-7})(.26162)$$

$$= .4899 \text{ MPa}$$

Landing:

$$\sigma = N/A + Mc/I$$

$$= (.8742)(.26162)/(2926 \times 4.16 \times 10^{-7})$$

$$= 187.8 \text{ MPa}$$

$$\tau = (25.05)(.00306) / (2926 \times 4.16 \times 10^{-7})(.26162)$$

$$= 240.7 \text{ MPa}$$

Stress Transformation:

Stress transformation refers to the method of determining normal and shear stresses acting on different planes at a point within a material. This is critical in understanding how materials behave under various loading conditions, particularly when subjected to complex forces. Using the applied loads that act on the Avionics box and by extension the supporting structure, we can analyze the stress transformation that we can expect to see when extreme circumstances are experienced.

We sought to consider the principal stresses derived from the maximum and minimum normal stress, and the shear stress to ensure that our supporting structure is sufficient to withstand the expected conditions. Without this consideration, there is a risk that the material or the structure could be insufficient to support the box.

Using Mohr's circle, we calculated the maximum normal and shear stress experienced by the cross section of the supporting structure so that we can definitively tell if the chosen material is capable of meeting those stress thresholds the system requires.

Takeoff:

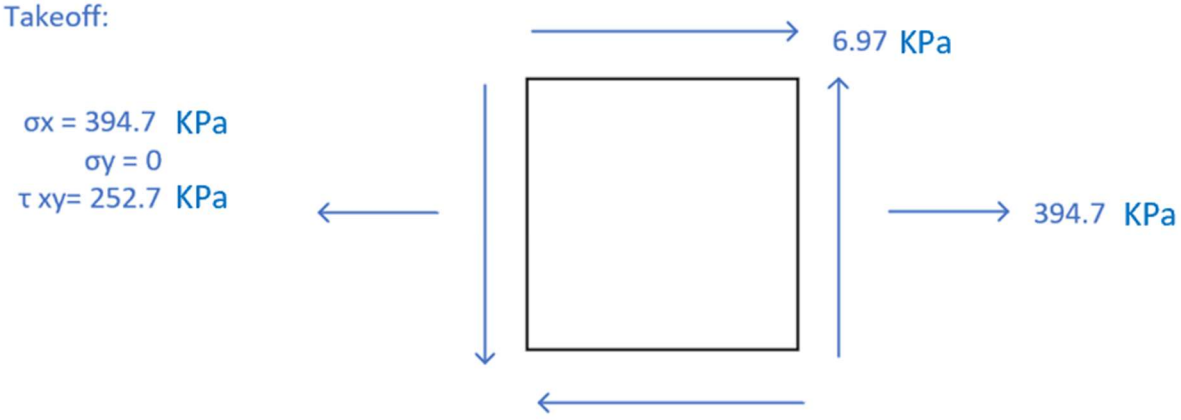

$\sigma_{avg} = (\sigma_x + \sigma_y)/2$

$= (394.7 + 0)/2$

$= 197.4$ KPa

$R = \sqrt{[((\sigma_x - \sigma_y)/2)^2 + \tau_{xy}^2]}$

$= \sqrt{[(197.4)^2 + (252.7)^2]}$

$= 370.7$

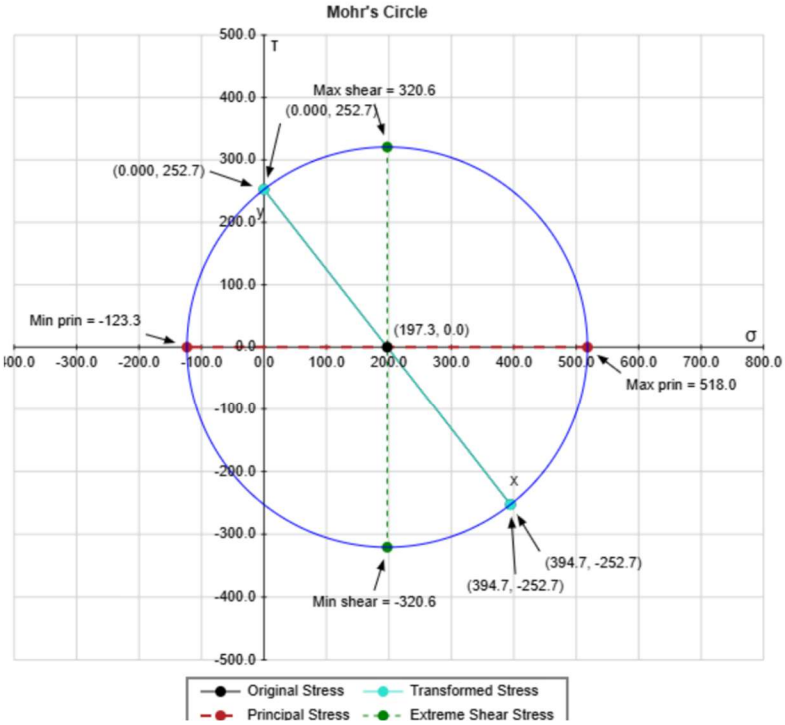

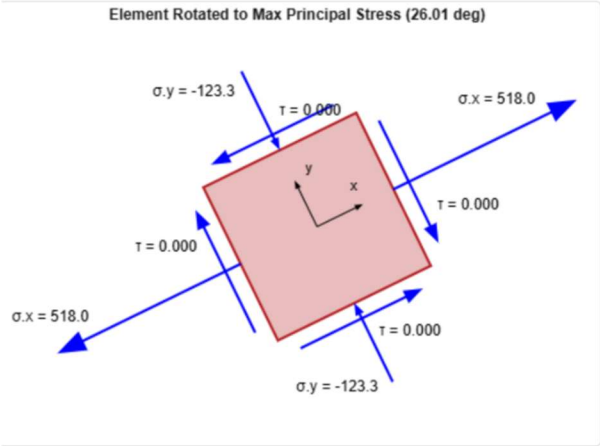

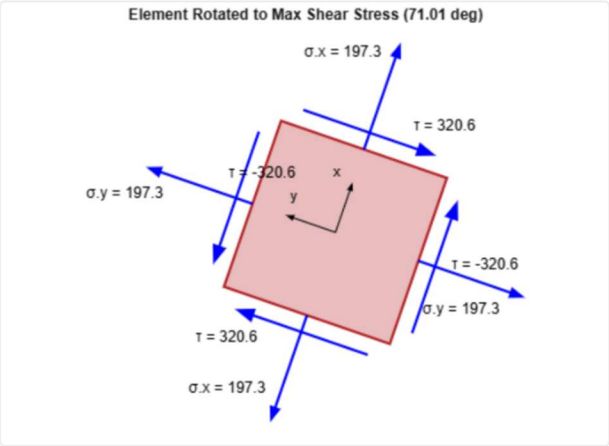

Level Flight:

σx = 1.63 KPa

σy = 0

τ xy= .4899 KPa

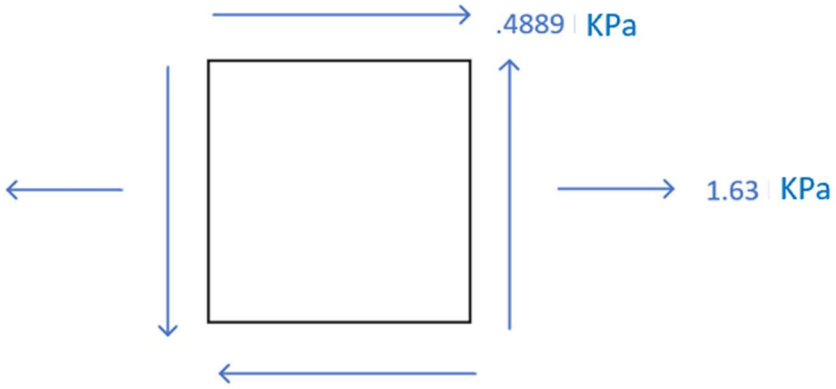

σavg = (σx + σy)/2

= .815 KPa

R = √ [((σx - σy)/2)^2 + τ xy^2]

= .951

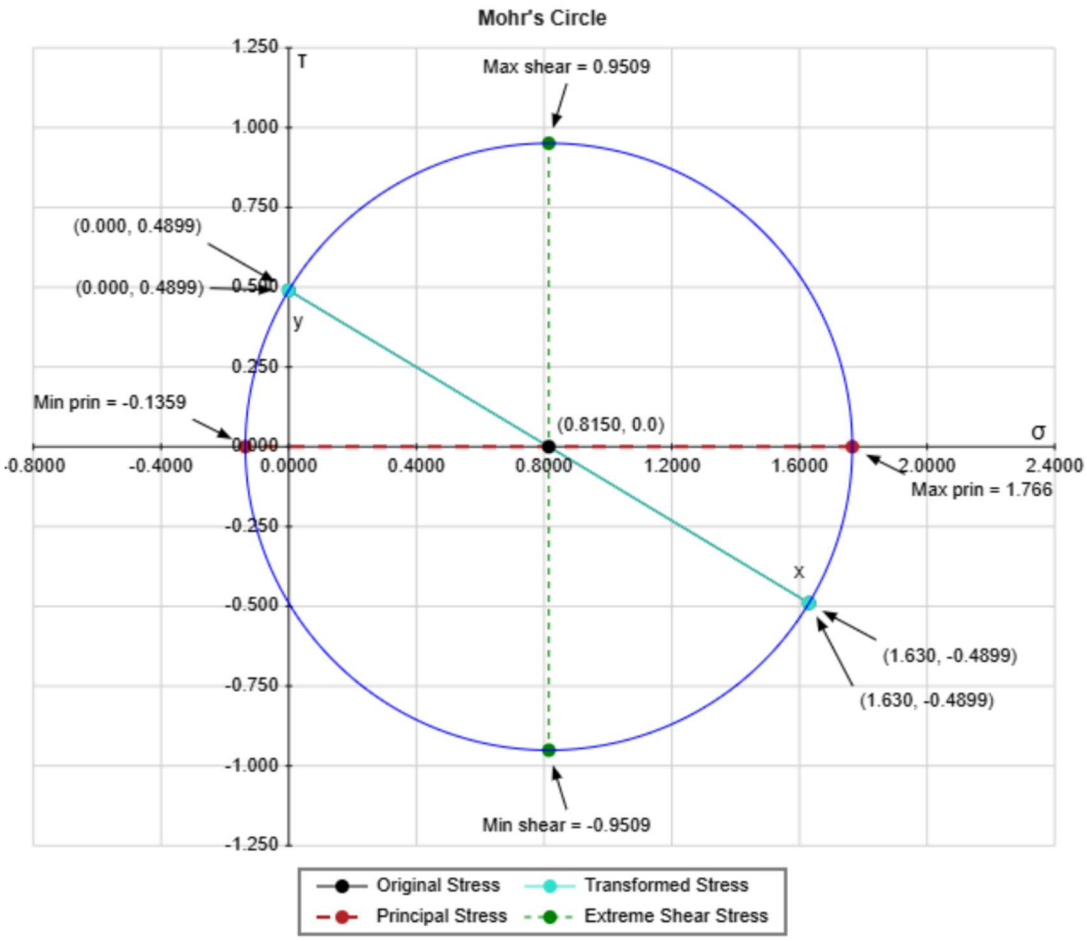
Mohr's Circle
T
σ
Max shear = 0.9509
Min shear = -0.9509
(0.000, 0.4899)
(0.000, 0.4899)
y
Min prin = -0.1359
(0.8150, 0.0)
Max prin = 1.766
x
(1.630, -0.4899)
(1.630, -0.4899)
1.250
1.000
0.750
0.500
0.250
0.0000
-0.250
-0.500
-0.750
-1.000
-1.250
-0.8000
-0.4000
0.0000
0.4000
0.8000
1.2000
1.6000
2.0000
2.4000
Original Stress
Transformed Stress
Principal Stress
Extreme Shear Stress

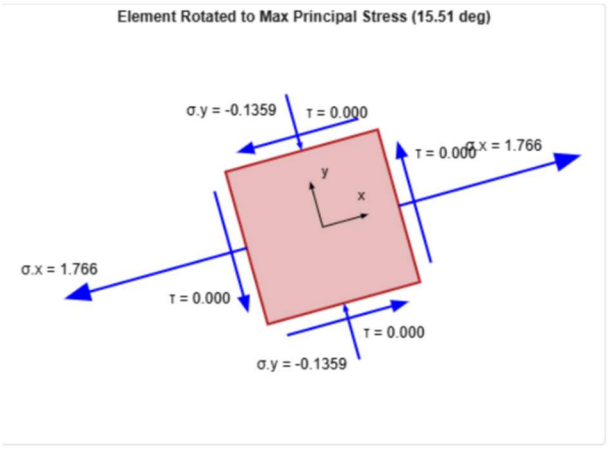
Element Rotated to Max Principal Stress (15.51 deg)
σ.y = -0.1359
τ = 0.000
τ = 0.000
σ.x = 1.766
σ.x = 1.766
τ = 0.000
τ = 0.000
σ.y = -0.1359
y
x

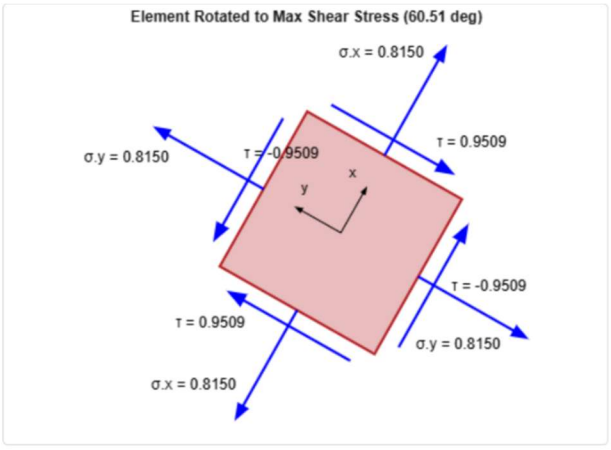
Element Rotated to Max Shear Stress (60.51 deg)
σ.x = 0.8150
σ.y = 0.8150
τ = -0.9509
τ = 0.9509
τ = -0.9509
τ = 0.9509
σ.y = 0.8150
σ.x = 0.8150
y
x

Conclusion and Suggestions:

Based on the initial design and the calculated forces and stresses during different flight conditions (such as taxiing, takeoff, turbulence, and landing), the mounting structure will need to be thoroughly evaluated against the material's strength limits for both normal and shear stresses. The initial design would fulfill the strength requirements.

However, if stress levels approach or exceeds the yield or ultimate strength of the material, modifications will be necessary to ensure structural integrity. Potential improvements include selecting a higher-strength material, adjusting the geometry of the mounting structure to better distribute loads, adding reinforcements, redesigning fasteners or joints for greater load-bearing capacity, and incorporating stress-relief features such as fillets at high-stress points. These modifications would help reduce the risk of failure and ensure the mounting system remains safe and effective under all operational loading conditions.

This report has comprehensively analyzed the various structural loads encountered by an aircraft throughout its operational phases—parking, taxiing, takeoff, turbulence, and landing—with special emphasis on their impact on support and mounting systems, particularly for components like avionics boxes. By treating static load as a foundational baseline, we were able to assess how additional dynamic forces such as acceleration, vibration, wind, and shear affect structural integrity at different moments in flight. Among these, landing emerged as the most critical phase, where combined vertical and horizontal forces can significantly amplify the loading on the aircraft’s structure and must be thoroughly considered in design.

This project significantly enhanced our understanding of solid mechanics, especially in applying core principles like shear and bending moment analysis, stress transformation, and inertial loading to a complex, real-world system. Through moment and shear diagrams, we directly connected classroom concepts with practical structural design considerations. Utilizing tools like SolidWorks and Mohr’s Circle allowed us to simulate and validate structural responses, reinforcing the importance of theoretical knowledge in engineering practice. Overall, this work bridged the gap between abstract concepts and their tangible applications in aerospace design, deepening both technical competence and appreciation for the complexity of real-world engineering systems.

Sources:

Aerodynamic flutter on aircraft control surfaces. Raptor Scientific. (2023, June 14). https://raptor-scientific.com/news/resources/aerodynamic-flutter-on-aircraft-control-surfaces-testing-and-measurement-analysis/

Al-bess, L., & Khouli, F. (2024). Computational Investigation of a Flexible Airframe Taxiing Over an Uneven Runway for Aircraft Vibration Testing. *SAE International Journal of Aerospace, 17*(2), 165-185. https://doi.org/10.4271/01-17-02-0011

Federal Aviation Administration. (n.d.). *Acceleration in aviation: G-force*. Retrieved April 29, 2025, from https://www.faa.gov/pilots/safety/pilotsafetybrochures/media/acceleration.pdf

F-15 Eagle. Air Force. (n.d.). https://www.af.mil/About-Us/Fact-Sheets/Display/Article/104501/f-15-eagle/

The F-15 Eagle. (n.d.). https://media.defense.gov/2012/May/16/2001330012/-1/-1/0/AFD-120516-036.pdf

Kelvin-Helmholtz instability. Kelvin-Helmholtz Instability - an overview | ScienceDirect Topics. (n.d.). https://www.sciencedirect.com/topics/earth-and-planetary-sciences/kelvin-helmholtz-instability

Peters, J. (2019, October 21). *Causes of aircraft vibrations: ACES systems: Aviation Track and balance*. ACES Systems. https://www.acessystems.com/top-three-causes-of-aircraft-vibrations/

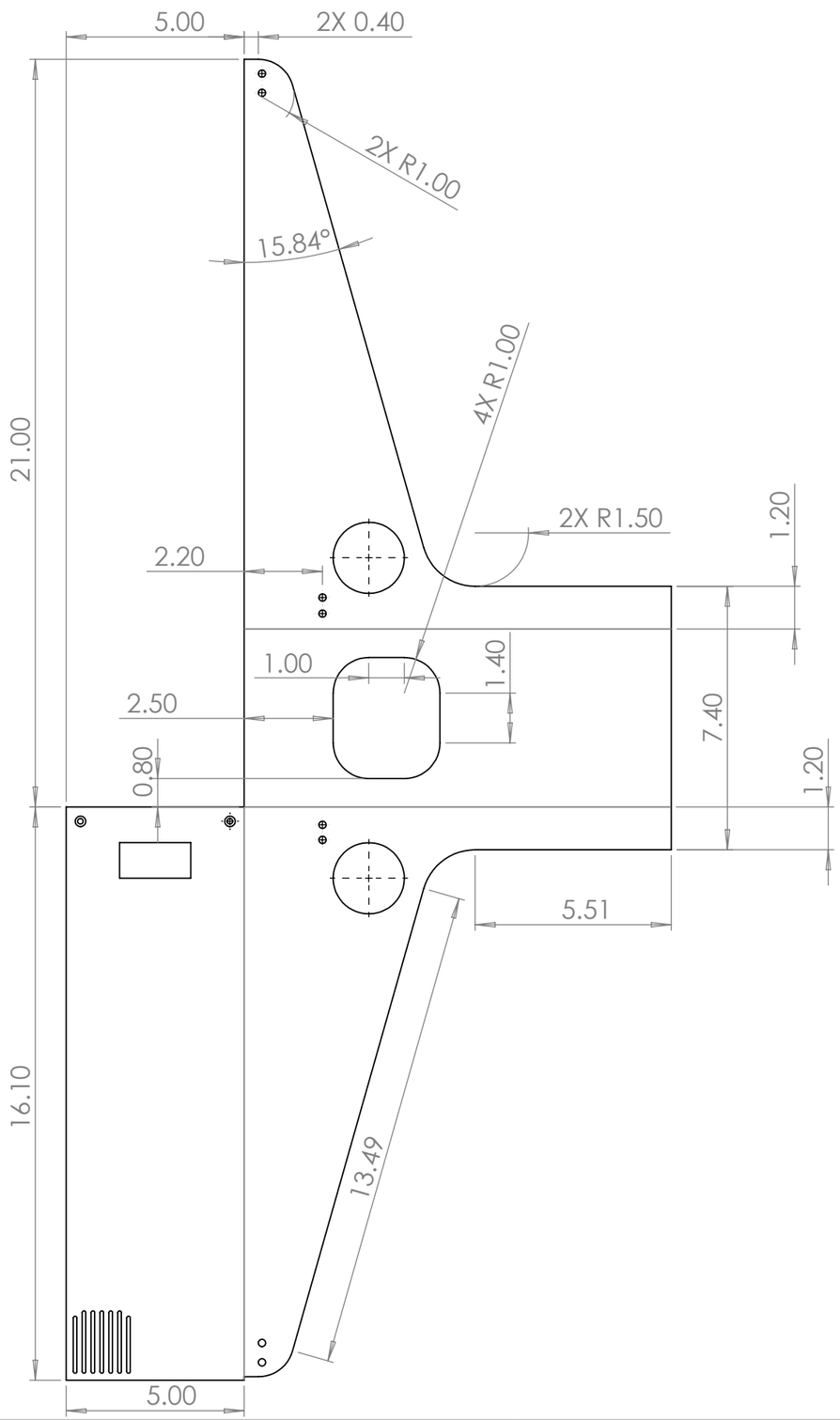

REVISIONS				
ZONE	REV.	DESCRIPTION	DATE	APPROVED BY TEAM
D1	A	SHEET METAL VERSION OF THE AVIONICS BOX MOUNT	4/27/2025	YES

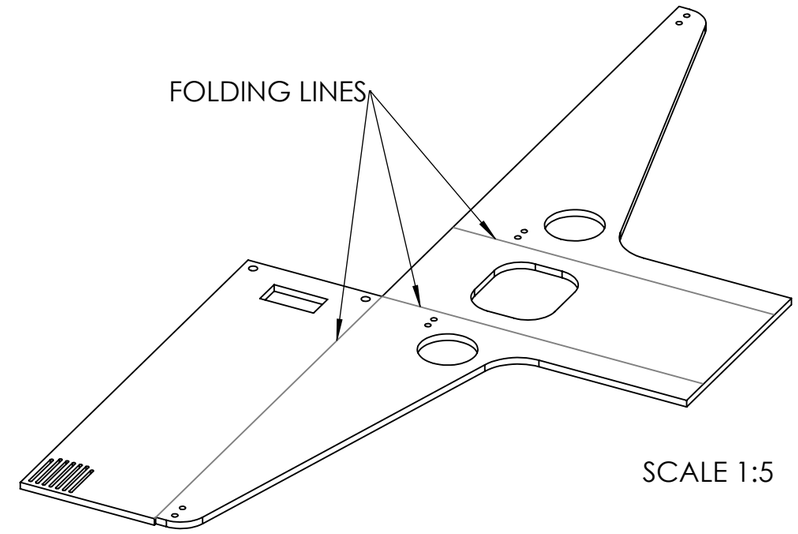

SCALE 1:5

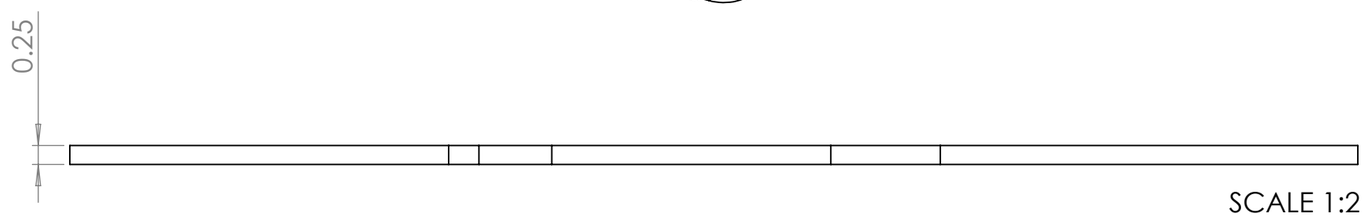

SCALE 1:2

WEIGHT 2.23lb

SURFACE AREA 533.90in^2

DO NOT SCALE DRAWING

UNLESS OTHERWISE SPECIFIED DIMENSIONS ARE IN INCHES
.XX = ±.01- ANGULAR = ±1°
.XXX = ±.005-
SURFACE FINISH

DRAWN BY Clancy Crawford

DATE Sunday, April 27, 2025 9:59:16 PM

COMMENTS:

ES202-ES305-2501-004

TITLE:

2 Dimensional Avionics Box for Sheet Metal

SIZE	DWG. NO.	REV
B	1	A

SCALE: 1:10 SHEET 1 OF 2

REVISIONS				
ZONE	REV.	DESCRIPTION	DATE	APPROVED BY TEAM
D1	A	SHEET METAL VERSION OF THE AVIONICS BOX MOUNT	4/27/2025	YES

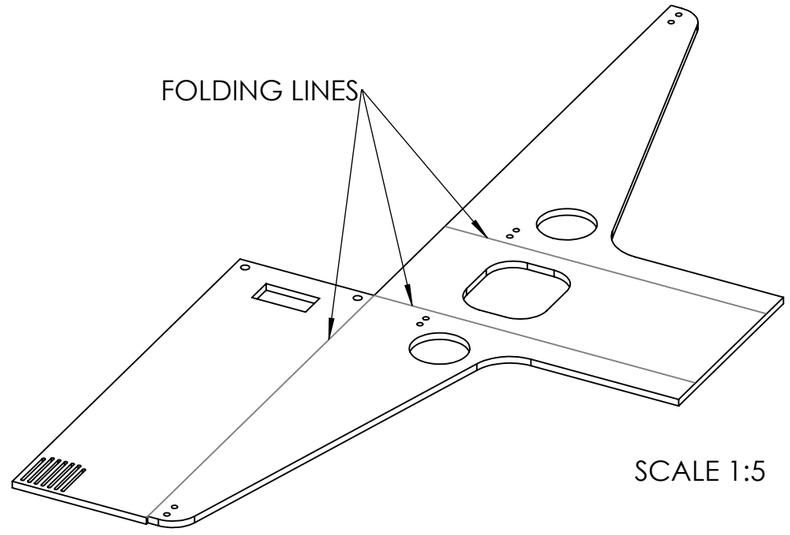

SCALE 1:5

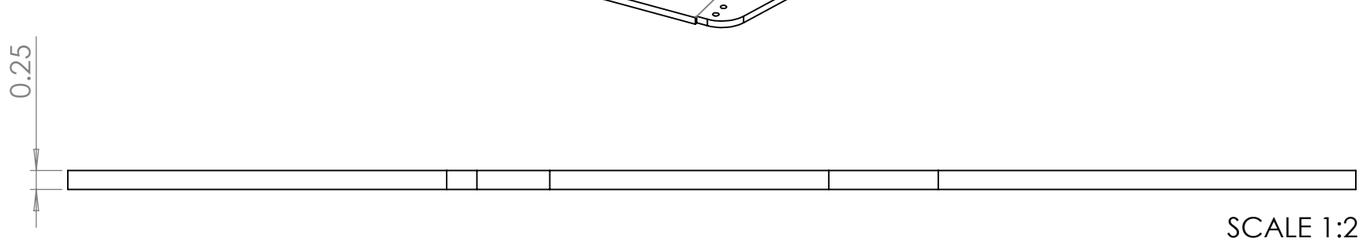

SCALE 1:2

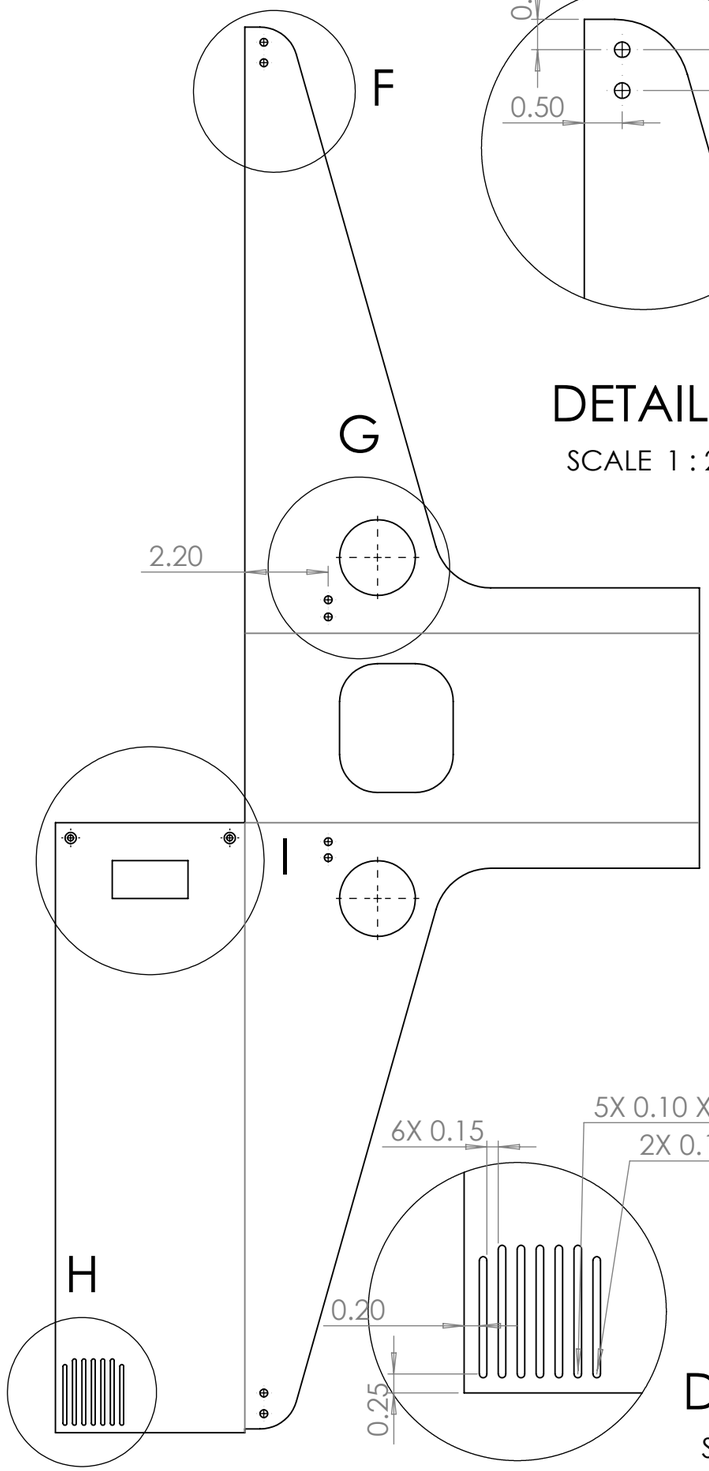

DETAIL F

SCALE 1 : 2

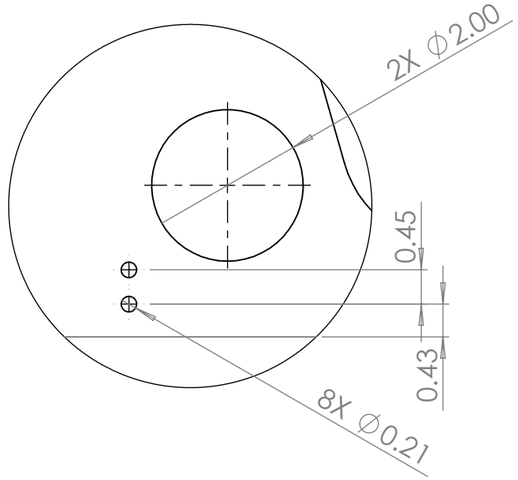

DETAIL G

SCALE 1 : 2

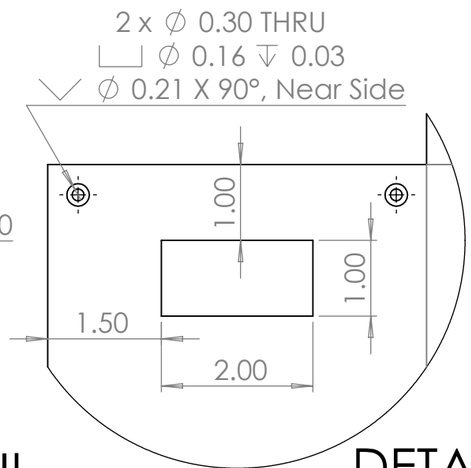

DETAIL H

SCALE 1 : 2

DETAIL I

SCALE 1 : 2

PROPRIETARY AND CONFIDENTIAL

THE INFORMATION CONTAINED IN THIS DRAWING IS THE SOLE PROPERTY OF <INSERT COMPANY NAME HERE>. ANY REPRODUCTION IN PART OR AS A WHOLE WITHOUT THE WRITTEN PERMISSION OF <INSERT COMPANY NAME HERE> IS PROHIBITED.

UNLESS OTHERWISE SPECIFIED DIMENSIONS ARE IN INCHES
.XX = ±.01- ANGULAR = ±1°
.XXX = ±.005-
SURFACE FINISH

DRAWN BY Clancy Crawford

DATE Sunday, April 27, 2025 9:59:16 PM

WEIGHT 2.23lb

SURFACE AREA 533.90in^2

DO NOT SCALE DRAWING

COMMENTS:

ES202-ES305-2501-004

TITLE:

2 Dimensional Avionics Box for Sheet Metal

SIZE	DWG. NO.	REV
B	2	A
SCALE: 1:4		SHEET 2 OF 2

ITEM NO.	PART NUMBER	DESCRIPTION	QTY.
1	Connector Plate with flush back		1
2	Flat Bottom w flush back		1
3	Side with flush back		2
4	Supports w flush back		2

REVISIONS				
ZONE	REV.	DESCRIPTION	DATE	APPROVED BY TEAM
1F	A	See Sheet1	4/27/25	YES

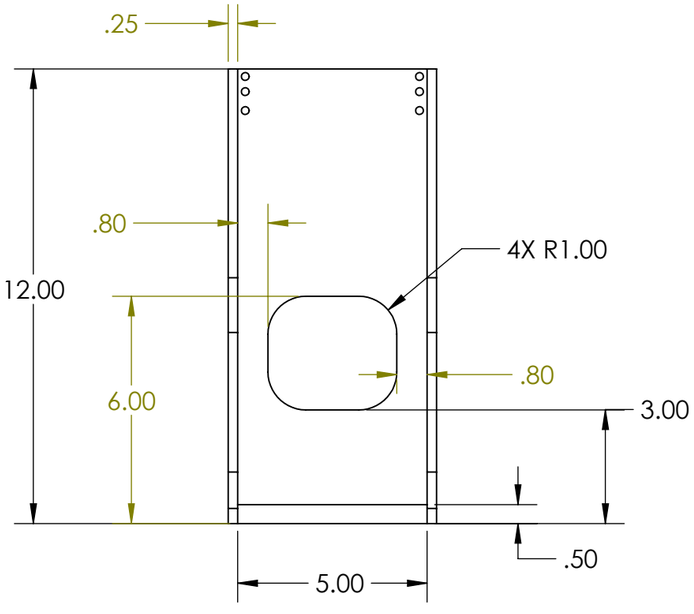

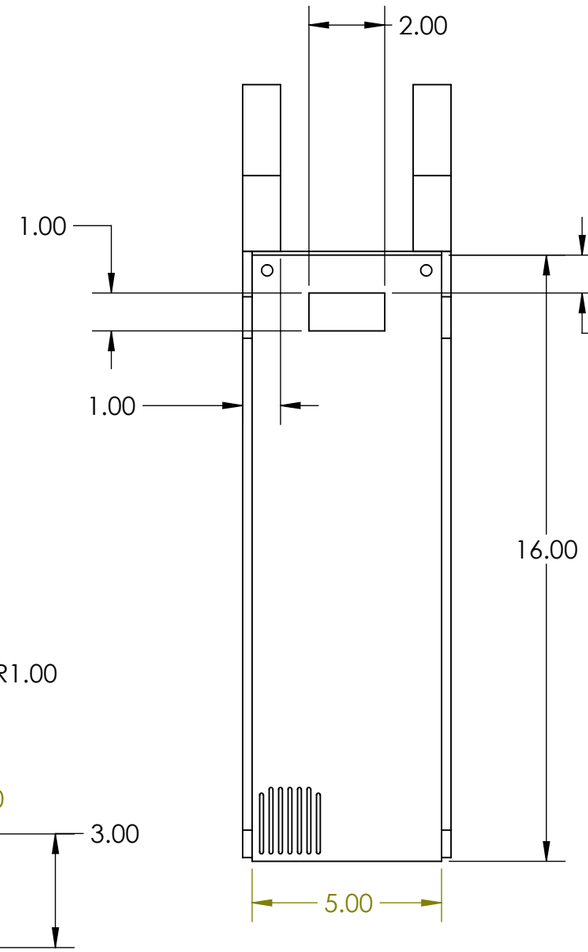

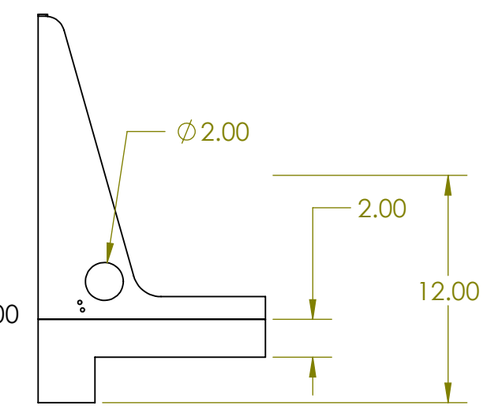

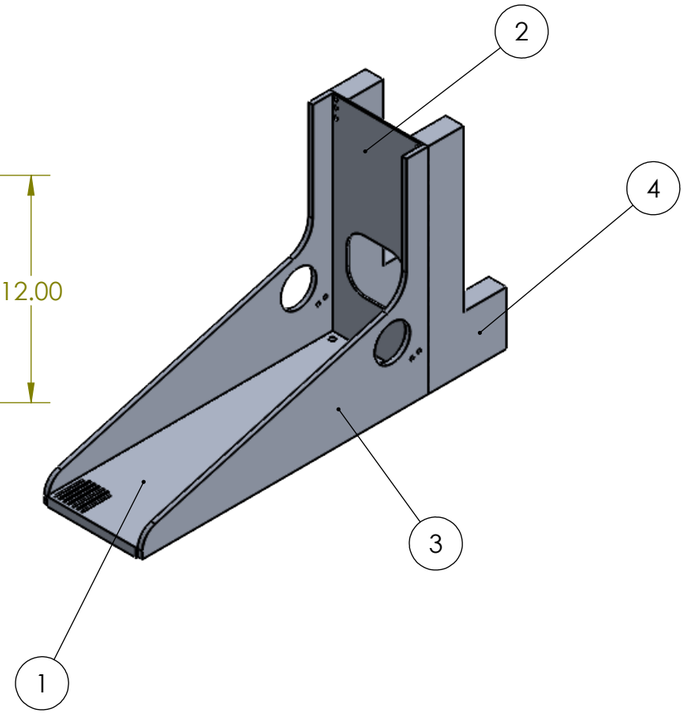

*NOTICE: THIS SHEET IS TO EXCLUSIVELY HELP WITH VISUALIZING THE SET UP OF THE AVIONICS BOX. THE ACTUAL MOUNT IS 2D.

UNLESS OTHERWISE SPECIFIED DIMENSIONS ARE IN INCHES
.XX = ±.01- ANGULAR = ±1°
.XXX = ±.005-

DRAWN BY Clancy Crawford

DATE 4/27/2025

WEIGHT 336.48lb

SURFACE AREA 1183.26in^2

DO NOT SCALE DRAWING

COMMENTS:

ES202-ES305-2501-A002

TITLE:

ASSEMBLY OF BOX

SIZE	DWG. NO.	REV
B	1	A

SCALE: 1:6 SHEET 1 OF 1

REVISIONS				
ZONE	REV.	DESCRIPTION	DATE	APPROVED BY TEAM
1G	A	ASSEMBLY OF BOX	4/27/2025	YES

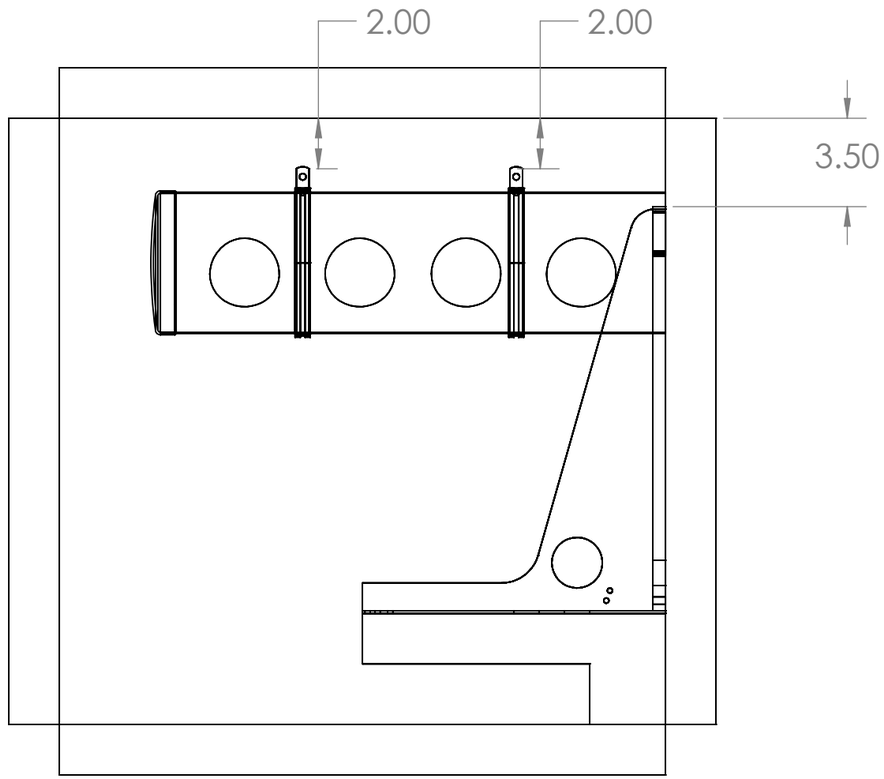

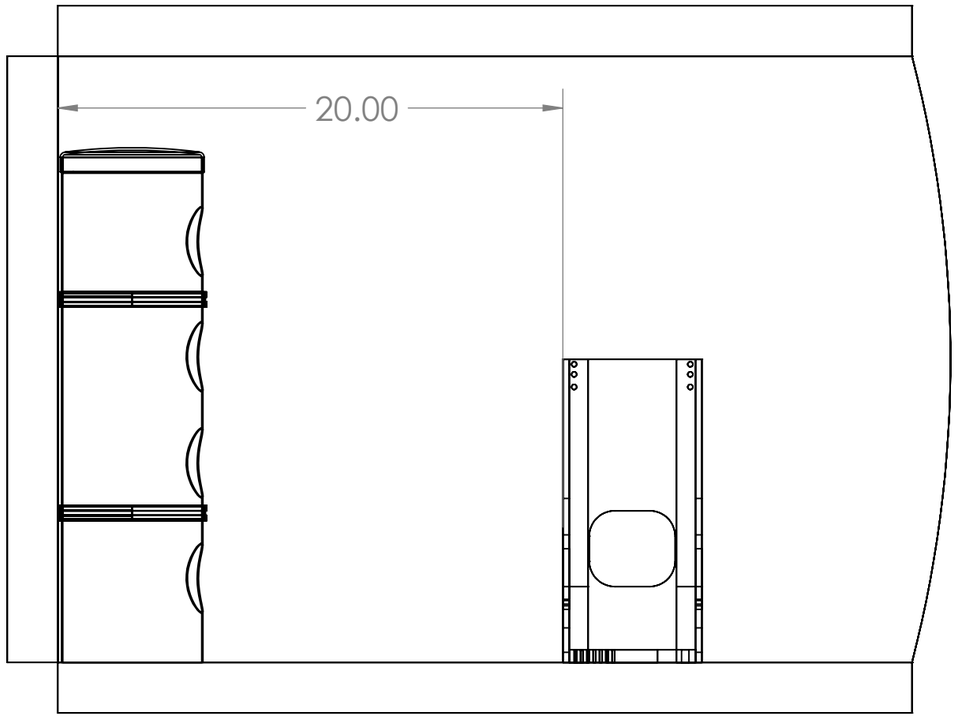

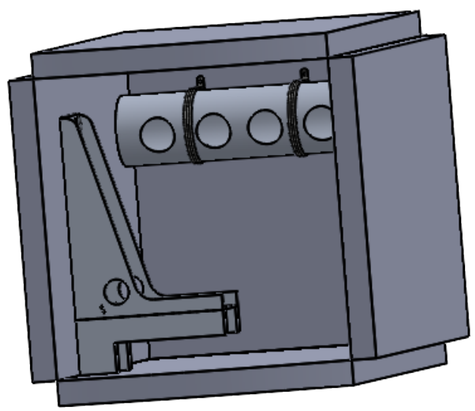

*NOTICE: THIS SHEET IS TO EXCLUSIVELY HELP WITH VISUALIZING THE SET UP OF THE AVIONICS BOX.

NOTE:
- THE BOTTOM OF THE FLUSH BACK ASSEMBLY IS COINCIDENT WITH THE BOX.
- THE PIPE AND FLUSH BACK ASSEMBLY ARE COINCIDENT WITH THE SIDE OF THE BOX.
- THE PIPE IS RESTING IN THE CLAMPS.
- THE CLAMPS ARE COINCIDENT WITH THE BOX.

UNLESS OTHERWISE SPECIFIED DIMENSIONS ARE IN INCHES
.XX = ±.01- ANGULAR = ±1°
.XXX = ±.005-
SURFACE FINISH

DRAWN BY Clancy Crawford

DATE 4/27/2025

WEIGHT 336.48lb

SURFACE AREA 1183.26in^2

DO NOT SCALE DRAWING

COMMENTS:

ES202-ES305-2501-A002

TITLE:

ASSEMBLY OF BOX

SIZE	DWG. NO.	REV
B	1	A

SCALE: 1:8 SHEET 1 OF 2

ITEM NO.	PART NUMBER	DESCRIPTION	QTY.
1	BOX	A-ES202305-006	1
2	BOX LID	A-ES202305-007	1
3	PIPE 9056K727	THIN-WALL BUTT-WELD UNTHREADED PIPE FITTING	1
4	AVIONICS MOUNT	3D ASSEMBLY WITH FLUSH BACK	1
5	3225T11	VIBRATION-DAMPING LOOP CLAMP	2
6	PIPE CAP 45735K282	THIN-WALL BUTT-WELD UNTHREADED PIPE FITTING	1

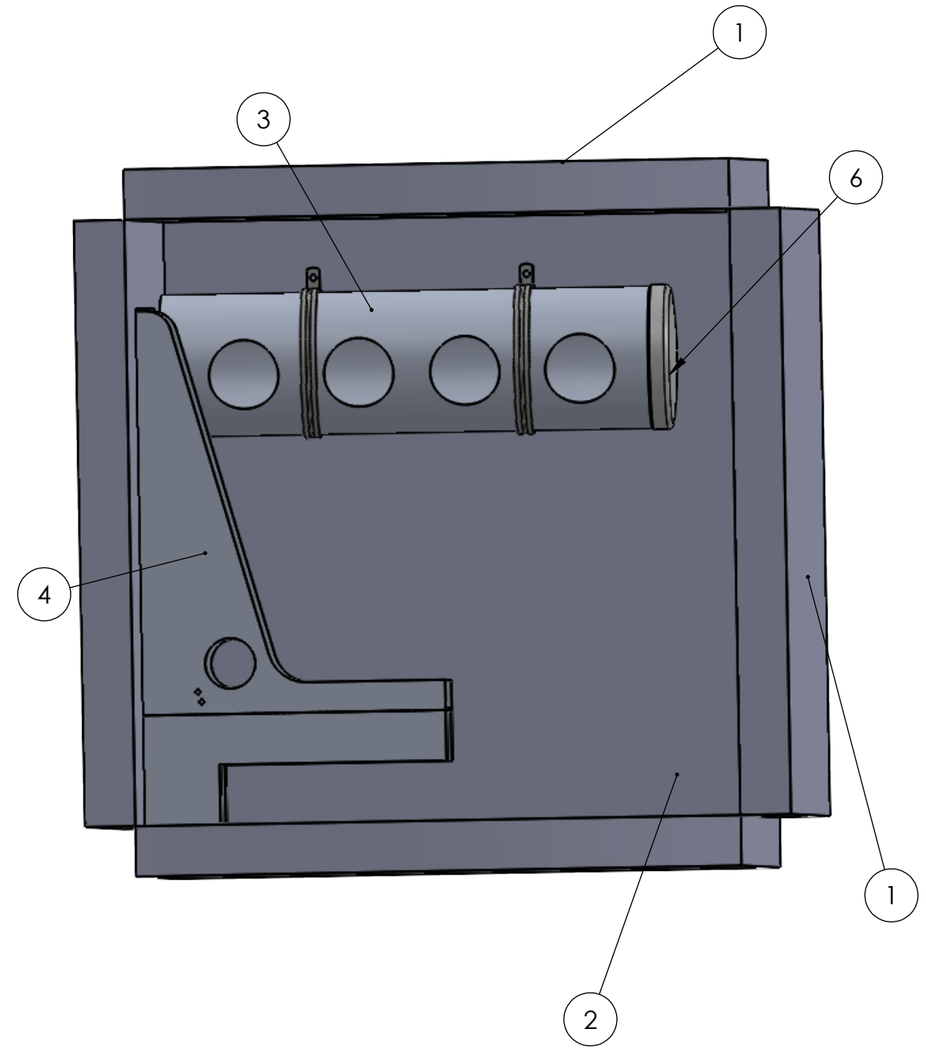

*NOTICE: THIS SHEET IS TO EXCLUSIVELY HELP WITH VISUALIZING THE SET UP OF THE AVIONICS BOX.

UNLESS OTHERWISE SPECIFIED DIMENSIONS ARE IN INCHES
.XX = ±.01- ANGULAR = ±1°
.XXX = ±.005-

DRAWN BY Clancy Crawford

DATE 4/27/2025

COMMENTS:

WEIGHT 336.48lb

SURFACE AREA 1183.26in^2

DO NOT SCALE DRAWING

ES202-ES305-2501-A002

TITLE:

ASSEMBLY OF BOX

SIZE	DWG. NO.	REV
B	2	A

SCALE: 1:6 SHEET 2 OF 2

Thermodynamics Final Report

ES – 305 R. Rodriguez

Kendall Pielin, Craig Slovensky, Clancy Crawford, and Hayden O’Shea

Adiabatic Wall Temperature:

Known: A F-22 is flying at a Mach number of 2.2 at an altitude of 30,000 feet above sea level. Consider the aircraft's external air temperature and velocity relative to the still air in this scenario.

Find: Determine the air temperature on the surface of a stationary object on the aircraft door where the air is considered stagnant due to boundary layer effects.

Schematic:

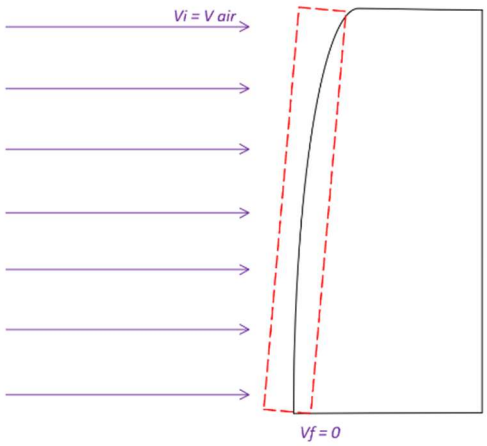

Properties:

State 1; Air	
$T_{alt} = 59 - (.00356620 \cdot 30000\ ft) = -47.9°F = 412.1°R$	❶
$P_{alt} = (14.969\ psia)(1 - (6.8754 \cdot 10^{-6} \cdot z)^{5.2559} \cong 14.969\ psia$	❷
$h_1 = 98.41\ Btu/lbm$	❸

Assumptions: The air will be stagnant on the outside of the door, steady state, streamline flow, neglect changes in potential energy, no additional work or heat is added to the system, air acts as an ideal gas, isentropic.

Solution:

$$mach = \frac{V}{\sqrt{KRT}} \rightarrow V_{air} = mach \cdot \sqrt{KRT}$$ ❹

$$V_{air} = (2.2)(\sqrt{(1.4)\left(\frac{1545}{28.96} \cdot \frac{ft \cdot lbf}{lbmol\ °R}\right)(412.1°R)\left(32.2\frac{ft}{s}\right)} = 2190.18\ ft/s$$

$$\frac{dE_{cv}}{dt} = \dot{Q} - \dot{W} + \dot{m}\left[h_1 - h_2 + \frac{{v^2}_1 + {v^2}_2}{2} + g(z_1 - z_2)\right]$$ ❺

$$h_2 = h_1 + \frac{{v_1}^2}{2} = \left(98.41\frac{Btu}{lb}\right) + \left(\frac{(2190.18)^2\frac{ft^2}{s^2}}{2}\right)\left(\frac{lbf}{\left(32.2lbm \cdot \frac{ft}{s^2}\right)}\right)\left(\frac{1Btu}{778lbf \cdot ft}\right)$$

$$h_2 = 194.15\frac{Btu}{lbm} \rightarrow T = 809.59\ °F$$ ❸

Comments: While this analysis assumes the air at the aircraft surface is fully stagnant due to boundary layer effects, in reality, the boundary layer may retain some motion, and turbulence or surface roughness could prevent complete conversion of kinetic energy into internal energy.

The assumption of steady-state flow eliminates the possibility of transient effects, such as those caused by changes in altitude, speed, or flight maneuvering, which can significantly impact local temperature and pressure. Treating the flow as isentropic neglects the presence of shock waves, which are likely at Mach 2.2 and would increase entropy, thereby reducing the actual stagnation temperature relative to ideal predictions.

Total Heat Transfer:

Known: A sealed and well-insulated compartment is exposed to two internal sources of heat: conduction through an aluminum door and electrical power dissipation from an internal electronic box. The door is constructed from Aluminum 6061-T6, with a uniform thickness of 0.25 inches and a surface area of 638.1 in^2. The outside surface of the door is exposed to an external temperature of 220°F, while the interior surface is at 200°F. The electronic box operates at a current of 15.5 amps and a voltage of 28 volts.

Find: The total heat transfer to the compartment.

Assumptions: Uniform material and thickness, linear temperature gradient across the width of the door, 100% efficiency of electrical energy to heat, well insulated compartment

Schematic:

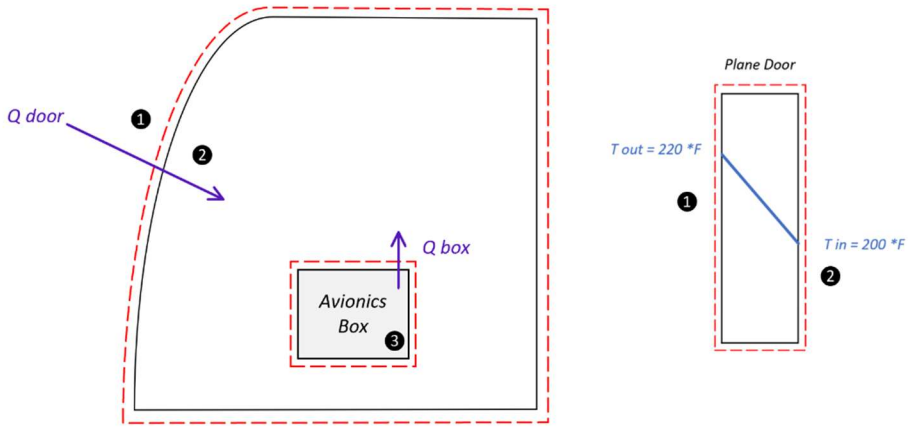

Properties:

State 1; Al 6061-T6	State 2; Al 6061-T6	State 3; Box
$T_{out} = 220°F$ $k = 96.51 \frac{Btu}{ft \cdot hr \cdot °F}$ ❻	$T_{in} = 200°F$ $k = 96.51 \frac{Btu}{ft \cdot hr \cdot °F}$	$I = 15.5\ amps$ $V = 28\ volts$ $\eta_{th} = 1.00$

Solution:

$$Q_{door} = -kA\frac{dt}{dx} = -kA\Delta T$$ ❼

$$Q_{door} = -\left(96.51\frac{Btu}{ft \cdot hr \cdot °F}\right)(638.1\ in)\left(\frac{1\ ft}{144in^2}\right)\left(\frac{(200-220)°F}{(.25in)\left(\frac{1ft}{12in}\right)}\right)$$

$$Q_{door} = 410553.54\frac{Btu}{hr}$$

$$Q_{box} = \dot{W} = P = IV$$ ❽

$$Q_{box} = (15.5\ amps)(28\ volts) = 434\ watts$$

$$Q_{box} = (434\ watts)\left(\frac{1\frac{Btu}{hr}}{3.14\ watts}\right) = 1481.7\frac{Btu}{hr}$$

$$Q_{tot} = Q_{door} + Q_{box}$$

$$Q_{tot} = (410553.54 + 1481.7)\frac{Btu}{hr}$$

$$Q_{tot} = 412035.24\ Btu/hr$$

Comments: While this analysis assumes the door and the electrical box are the only sources of heat within the compartment, in reality, there could be additional contributions such as radiation from external surfaces, minor air leakage, or heat generation from other electronic components.

The assumption of linear temperature distribution across the door simplifies the conduction equation and allows for direct use of Fourier's Law in one dimension. However, this overlooks potential temperature variations due to non-uniform material properties, temperature-dependent conductivity, or localized hot spots on the door caused by uneven external exposure (e.g., sunlight or aerodynamic heating).

The assumption of perfect insulation eliminates any losses to the surrounding environment. In practical applications, even well-insulated systems experience some degree of heat leakage, especially through seams, fasteners, or mounting points, which could affect the internal energy balance over time.

Lastly, assuming that all electrical power from the box is converted into heat may slightly overestimate its thermal contribution, as some energy could be used for light, motion, or stored in capacitors, depending on the box's function.

Pipe Diameter and Mass Flow Calculations:

Known: The air in the compartment has to be maintained at 160*F and 15 psig.

Assumptions: Steady state, no additional work on the system, well insulated, neglect changes in potential and kinetic energy, incompressible flow.

Schematic:

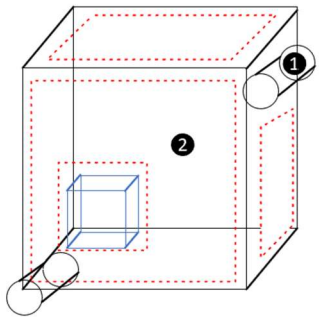

Properties:

State 1; Air	State 2; Air
T = 40*F P = 15 psig = 19.7 psia h = 119.48 Btu/lb	T = 160*F = 620*F P = 15 psig = 19.7 psia h = 148.28 Btu/lb

Solution:

$$Mach = \frac{V}{V_s} \rightarrow V = mach \cdot V_s = (.2)\left(1096\frac{ft}{s}\right) = 219.2\frac{ft}{s} \quad ❹$$

$$\rho = \frac{P}{R \cdot T} = \frac{(19.7psia)\,(144in^2)}{\left(\frac{1545}{28.96}\right)\frac{ft \cdot lbf}{lbmol\,°R}(500°R)} = .1063\frac{lbm}{ft^3} \quad ❾$$

$$\frac{dE_{cv}}{dt} = \dot{Q} - \dot{W} + \dot{m}\left[h_1 - h_2 + \frac{{v^2}_1 + {v^2}_2}{2} + g(z_1 - z_2)\right] \quad ❺$$

$$\dot{m} = -\frac{\dot{Q}}{h_1 - h_2} = -\frac{(412035.24)\frac{Btu}{hr}}{(119.48 - 148.28)\frac{Btu}{lbm}} = 14306\frac{lbm}{hr} = 3.974\frac{lbm}{s}$$

$$\dot{m} = \rho AV \rightarrow A = \frac{\dot{m}}{\rho V} = \frac{(3.974)\frac{lb}{s}}{\left(.10634\frac{lbm}{ft^3}\right)(219\frac{ft}{s})} = .1706\,ft^2$$

Additional Calculations:

$$d_i = \sqrt{\frac{4A}{\pi}} = .466\ ft \cong 5.5\ in$$

$$A = .1706\ ft^2 \cdot \frac{144 in^2}{1\ ft^2} = 24.56\ in^2$$

$$A_{hole} = \frac{A}{\#\ of\ holes} = \frac{24.56}{4} = 6.14\ in^2$$

$$d_{hole} = \sqrt{\frac{A_{hole} \cdot 4}{\pi}} = \sqrt{\frac{6.14 \cdot 4}{\pi}} \cong 2.75\ in$$

Comments: Since the flow is assumed to incompressible you can solve for the velocity of the air flowing into the compartment by using a Mach number of .2. The density variation at this level would be relatively negligible.

Using the First Law of Thermodynamics and the assumptions made you can solve the conservation of energy equation for an open system for mass flow. Relating this equation to the mass flow equation of volumetric flow rate times density you can solve for the area of the pipe.

If you reduce the size of each pipe outlet but increase the number of outlets, the total combined area of all outlets must stay the same to maintain the same flow rate. This ensures the system can handle the same volume of fluid.

Pipe Properties:

Known: The pipe is required to support a 125lbf, 10 inches from the wall. There are P-Clamps 1/3 and 2/3 the length of the pipe. The cap on the end of the pipe is welded together.

Find: Required supports, safety factor, and outside diameter.

Schematic:

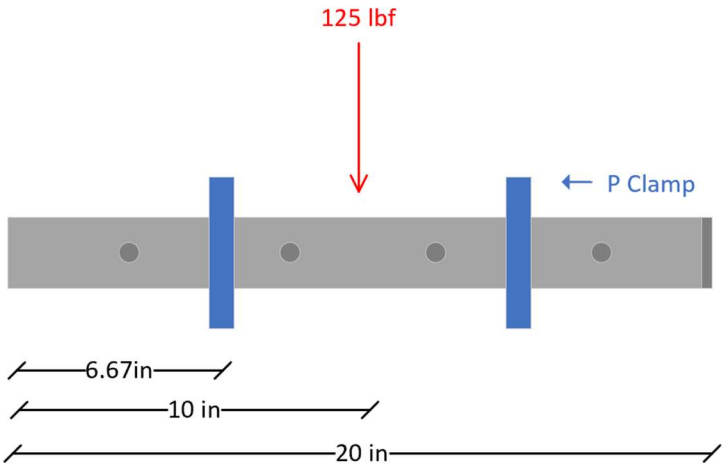

Assumptions: Material is consistent, clamps are identical

Properties:

Pipe ; Aluminum 6061-T6	
$\sigma_y = 40000\ psi$ $d_i = 5.5\ in.$ $d_o = 5.6\ in.$ $t_w = .05\ in.$	❿

Solution:

$M = F\ x\ d = (125\ lbf)(3.33) = 412.25\ lbf \cdot in$ ⓫

$I = \frac{\pi(d_o{}^4 - d_i{}^4)}{64} = \frac{\pi(5.6^4 - 5.5^4)}{64} = 3.36\ in^4$ ⓬

$\sigma = \frac{M \cdot c}{I} = \frac{(412.25 lbf \cdot in) \cdot (2.8\ in)}{3.36\ in^4} = 346.9\ lbf/in^2$ ⓭

$SF = \frac{\sigma_y}{\sigma_a} = \frac{40000\ psi}{346.9\ psi} = 115.3$

Additional Diagrams:

Fig 1.1

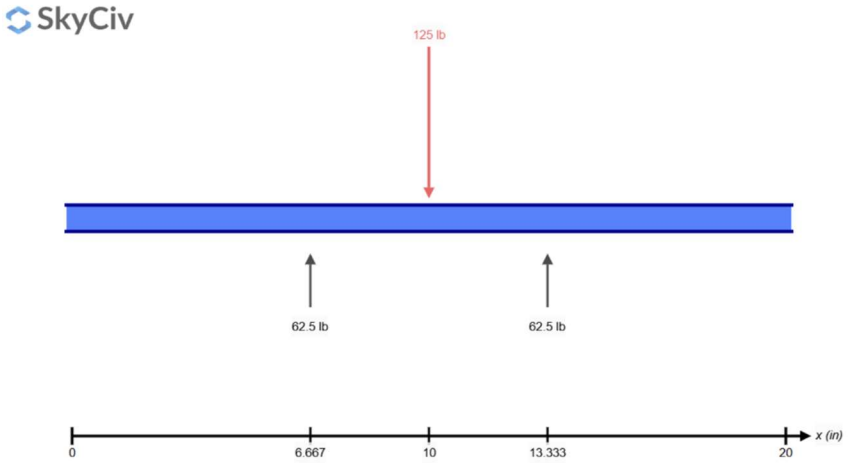

Fig 1.2

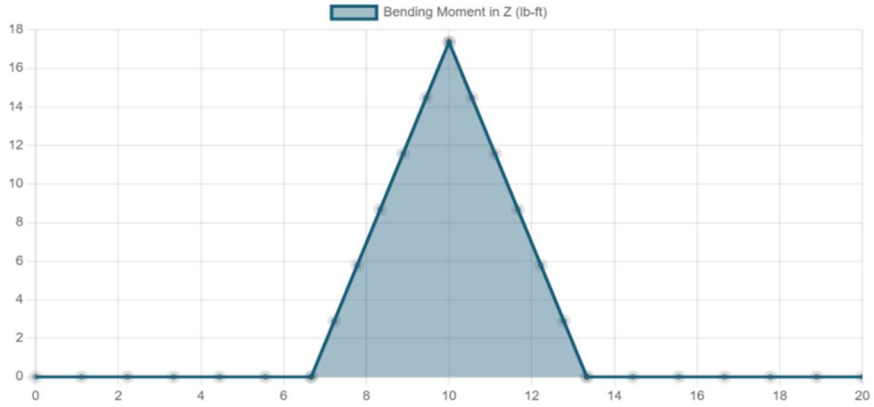

Fig 1.3

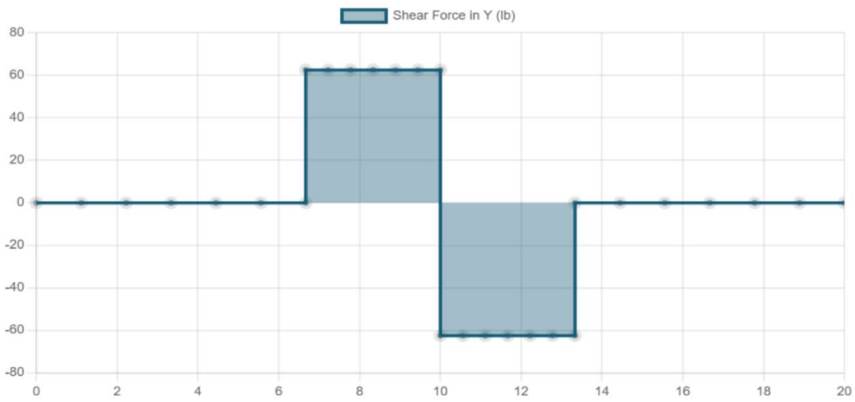

Comments: To minimize deflection under load, the hanging pipe is supported by two P-clamps spaced at one-third intervals along its total length. The pipe extends 20 inches from the wall, with the first clamp positioned 6.67 inches from the wall and the second clamp placed another 6.67 inches further along the pipe. This evenly distributed support helps prevent excessive bending and reduces the risk of the pipe exceeding its yield strength.

While a large safety factor like 115.3 guarantees a very safe design, it may not always be necessary for all applications. Aerospace engineers need to balance safety with efficiency, cost, and weight. A more typical safety factor, likely between 1.5 and 3, would suffice for most structural components, unless the design specifically requires additional reliability due to critical, high-risk factors. It's important to evaluate the trade-offs and adjust the safety factor according to the performance requirements and operating conditions of the system.

Conclusion: This project applied core principles of thermodynamics to analyze the thermal and fluid behavior in a compartment system in an F-22 aircraft. Through a series of structured calculations and justified assumptions, we determined the adiabatic wall temperature experienced by a stationary surface at Mach 2.2 to be approximately 809.6°F, accounting for energy conversion from high-speed airflow. We then evaluated the total heat transfer into a sealed compartment due to both conduction through an aluminum door and internal electrical dissipation, yielding a combined heat input of over 412,000 BTU/hr.

To maintain desired internal conditions of 160°F and 15 psig, we analyzed the necessary air mass flow rate and inlet area. The resulting design called for multiple airflow holes, each approximately 2.75 inches in diameter, ensuring steady-state temperature regulation. Lastly, structural integrity of the pipe system used for airflow distribution was validated using mechanical stress analysis. The calculated safety factor of 115.3 confirmed the aluminum pipe's suitability for the load conditions, emphasizing both reliability and overdesign margin.

Overall, this analysis highlights the importance of integrating thermodynamic and structural considerations in aerospace systems design. Realistic assumptions, while simplifying complex systems, also illustrate the need for careful interpretation of results, especially under extreme conditions such as supersonic flight. The methods and findings in this report offer a practical framework for future thermal management and structural planning in high-performance aircraft environments.

References:

❶ ASHRAE. (2021). *ASHRAE Handbook – Fundamentals* (Chapter 1: Psychometrics). American Society of Heating, Refrigerating and Air-Conditioning Engineers, Inc. : Temperature at Altitude Equation

❷ ASHRAE. (2021). *ASHRAE Handbook – Fundamentals* (Chapter 1: Psychometrics). American Society of Heating, Refrigerating and Air-Conditioning Engineers, Inc. : Pressure at Altitude Equation

❸ Moran, M. J., Shapiro, H. N., Boettner, D. D., & Bailey, M. B. (2020). *Fundamentals of engineering thermodynamics* (9th ed.). (Table A-22E, PG. 687) Wiley. : Properties for Air as an Ideal Gas

❹ Moran, M. J., Shapiro, H. N., Boettner, D. D., & Bailey, M. B. (2020). *Fundamentals of engineering thermodynamics* (9th ed.). (Chapter 9.13, PG. 353) Wiley. : Mach Number Ratio

❺ Moran, M. J., Shapiro, H. N., Boettner, D. D., & Bailey, M. B. (2020). *Fundamentals of engineering thermodynamics* (9th ed.). (Chapter 4.4, PG. 112) Wiley. : Conservation of Energy for a Control Volume

❻ National Institute of Standards and Technology. (n.d.). *Aluminum 6061-T6 (UNS A96061)*. U.S. Department of Commerce. Retrieved April 27, 2025 : Thermal Conductivity Constant

❼ Moran, M. J., Shapiro, H. N., Boettner, D. D., & Bailey, M. B. (2020). *Fundamentals of engineering thermodynamics* (9th ed.). (Chapter 2.4, PG. 39) Wiley. : Heat Transfer Modes – Conduction Eqn.

❽ Urone, P. P., & Hinrichs, R. (2020). *19.4 Electric power*. In *Physics*. OpenStax. : Electrical Power Eqn.

❾ Moran, M. J., Shapiro, H. N., Boettner, D. D., & Bailey, M. B. (2020). *Fundamentals of engineering thermodynamics* (9th ed.). (Chapter 3.12, PG. 90) Wiley. : Ideal Gas Eqn. of State

❿ Ferguson Perforating. (n.d.). *6061 aluminium alloy*. Ferguson Perforating. Retrieved April 26, 2025 : Yield Strength of Aluminum 6061 T-6

⓫ Kraige, L. G. (n.d.). *Moment of force*. Engineering Statics. Retrieved April 26, 2025 : Moment Equation

⓬ The Engineering ToolBox. (2008). *Area moment of inertia: Definitions, formulas & calculator*. Retrieved April 26, 2025 : Moment of Inertia of a Hollow Pipe

⓭ Nichols, A. (n.d.). *Beam design: Strength design for flexure* [PDF]. Texas A&M University. : Stress Equation

Figure 1.1 – 1.3 SkyCiv. (n.d.). *SkyCiv structural analysis software*. SkyCiv Engineering. : Moment and Shear Diagrams